Published in final edited form as:
Free Radic Biol Med. 2013 January ; 54: 51–61. doi:10.1016/j.freeradbiomed.2012.10.552.

Acute carbonyl stress induces occludin glycation and brain microvascular endothelial barrier dysfunction: Role for glutathione-dependent metabolism of methylglyoxal

Wei Li, **Ronald E. Maloney**, **Magdalena L. Circu**, **J. Steven Alexander**, and **Tak Yee Aw***
Department of Molecular and Cellular Physiology, Louisiana State University Health Sciences Center, Shreveport, LA 71130, USA

Abstract

We recently demonstrated that methylglyoxal (MG) induced apoptosis of brain microvascular endothelial cells (IHECs) that was preceded by glutathione (GSH) depletion. Here, we test the hypothesis that MG induces occludin glycation and disrupts IHEC barrier function, which is prevented by GSH-dependent MG metabolism. Exposure of IHECs to MG decreased transendothelial electrical resistance (TEER) in association with MG-adduct formation. A 65-kDa MG-glycated protein corresponded to occludin, which was confirmed by immunoprecipitation. Moreover, immunofluorescence staining showed that MG disrupted the architectural organization of ZO-1. Occludin glycation and ZO-1 disruption were prevented by *N*-acetylcysteine (NAC). Accordingly, TEER loss was abrogated by NAC (via GSH synthesis) and exacerbated by buthionine sulfoximine (BSO; GSH synthesis inhibitor). BSO treatment attenuated D-lactate production, consistent with a role for GSH in glyoxalase I-catalyzed MG elimination. Although MG increased reactive oxygen species (ROS) generation, the ROS scavengers tempol and tiron did not block barrier disruption. This suggests that endogenously generated ROS were unlikely to be a major cause of or did not reach a threshold to elicit barrier failure as elicited by exogenous hydrogen peroxide (300–400 μM). Immunohistochemistry revealed a lower percentage of microvessels stained with anti-occludin, but a higher percentage stained with anti-MG in diabetic rat brain compared to controls. Western analyses confirmed the decrease in diabetic brain occludin expression, but an increase in glycated occludin levels. These results provide novel evidence that reactive carbonyl species can mediate occludin glycation in cerebral microvessels and in microvascular endothelial cells that contribute to barrier dysfunction, a process that was prevented by GSH through enhanced MG catabolism.

Keywords

Methylglyoxal; Carbonyl stress; Endothelial GSH; Occludin glycation; Endothelial barrier function; Cerebral microvessels; Diabetes; Free radicals

It is well appreciated that reactive oxygen species (ROS)[1] are major contributors to attenuated endothelial-dependent vascular function in a variety of vascular pathologies [1].

*Corresponding author. Fax: +1 318 675 7393. taw@lsuhsc.edu (T.Y. Aw).

[1]*Abbreviations used:* BBB, blood–brain barrier; BSO, L-buthionine-(*S,R*)-sulfoximine; DHE, dihydroethidium; DHR, dihydrorhodamine 123; FITC, fluorescein isothiocyanate; FITC-150, FITC-Dextran 150; GPT, glutamic–pyruvate transaminase; GSH, glutathione; GSSG, glutathione disulfide; IHEC, immortalized human brain endothelial cell line; JAM, junction adhesion molecule; L-LDH, L-lactic dehydrogenase; MG, methylglyoxal; NAC, *N*-acetyl-L-cysteine; RCS, reactive carbonyl species; RIPA, radioimmunoprecipitation assay buffer; ROS, reactive oxygen species; STZ, streptozotocin; TEER, transendothelial electrical resistance.

However, a role for elevated reactive carbonyl species (RCS) in endothelial dysfunction is less well understood. Methylglyoxal (MG) is a highly reactive dicarbonyl species of α-oxoaldehyde produced mainly from cellular glycolytic intermediates and is a potent glycating agent. All macromolecules, viz., proteins, DNA, and lipids, can be glycated [2], and MG-induced formation of protein adducts (advanced glycation end products) with cell surface or intracellular targets has been shown to initiate tyrosine kinase signaling [3], mitochondrial dysfunction [4], and activation of the caspase cascade [5]. MG–protein adducts are generated by irreversible nonenzymatic modification of free amino groups of proteins, and carbonyl stress results from an imbalance between RCS levels, efficiency of scavenger and detoxification pathways, and accumulation of MG–protein adducts [2]. Moreover, the crosslinking reaction during MG amino acid glycation has been shown to yield the superoxide radical anion [6]. Consequently, protein damage by MG can be mediated not only via carbonyl stress through formation of protein carbonyls, but possibly also via oxidative stress through enhanced ROS formation [6]. However, the relative quantitative importance of MG-induced protein glycation and/or ROS generation in endothelial barrier function has not been previously explored.

Recently, MG-mediated glycation of extracellular matrix laminin and fibronectin and their accumulation in the endoneurium were shown to inhibit neurite outgrowth from sensory neurons, indicating that formation of protein carbonyls mediated the neurodegenerative pathology of the central nervous system [7]. Other studies have shown that MG can induce apoptosis in several cell types including Schwann cells [8], pheochromocytoma cells [9], and renal tubular cells [10], although the mechanism by which MG induced apoptotic death remains unclear. We found that MG-mediated apoptosis of human brain microvascular endothelial cells was initiated by an early disruption in the glutathione/glutathione disulfide (GSH/GSSG) status and was prevented by a restored cellular GSH state [11]. These findings demonstrated the vulnerability of brain endothelial cells to MG stress and the centrality of GSH in endothelial cell survival. Therefore, MG-induced carbonyl and/or oxidative stress could play an important role in neurovascular pathology, with the endothelium being an early and significant MG target site [11].

The endothelial monolayer that constitutes the blood–brain barrier (BBB) possesses no fenestrations and exhibits high transendothelial resistance, a property that is attributed to intercellular tight junctions between apposed endothelial cells [12]. Among the several tight-junctional proteins, occludin and cytoplasmic accessory zonula occludens proteins (ZO-1,−2, and −3) are pivotal in the regulation of endothelial monolayer electrical resistance, paracellular solute permeability, and normal barrier function [12]. Therefore, MG-mediated disruption of occludin and/or ZO-1 is expected to increase endothelial permeability, and the attenuation of MG stress would preserve barrier integrity. Cellular GSH can exhibit dual roles in MG detoxification, serving possibly as a reductant in the removal of superoxide anions generated by MG glycation reactions or as a cofactor in MG metabolism by the glyoxalase I/glyoxalase II system [13,14]. Evidence supporting a role for GSH in MG elimination comes from findings that physiological GSH levels maintain low intracellular levels of triosephosphate-derived MG (1–5 μM) [15]. Central to the maintenance of cellular GSH homeostasis is de novo synthesis, rate-limited by γ-glutamylcysteine ligase activity [16]. Thus, altered endothelial GSH synthesis could significantly influence MG effects on endothelial junctional integrity and barrier function.

In this study, we sought to investigate whether MG perturbs occludin and ZO-1 status and to determine the potential impact of such disruptions on endothelial barrier function. Given that GSH is central to MG elimination, we further examined how an alteration in GSH synthesis and GSH-dependent MG catabolism would affect MG–occludin formation and barrier integrity. Our working hypothesis, as summarized in Fig. 1, proposes that MG, probably

through glycation of occludin and/or disruption of ZO-1 structure, induces endothelial barrier dysfunction, an event that is prevented by endothelial GSH. Consistent with the hypothesis, we found that MG mediated a loss of barrier function in immortalized human brain microvascular endothelial cells (IHECs), a surrogate for the BBB endothelium in vivo in conjunction with increased MG–occludin adduct formation and disruption of ZO-1 organization. Although ROS production was detectable, MG-induced endothelial barrier dysfunction was ROS-independent. Notably, diabetic rat brains exhibited decreased total occludin and elevated glycated occludin contents, as well as fewer occludin-positive, but more MG-positive, cerebral microvessels.

Methods

Reagents

The following reagents were purchased from Sigma (St. Louis, MO, USA): MG, *N*-acetyl-L-cysteine (NAC), L-buthionine-(*S,R*)-sulfoximine (BSO), insulin-transferrin sodium selenite solution, fluorescein isothiocyanate (FITC), FITC–Dextran 150, dihydrorhodamine 123 (DHR), dihydroethidium (DHE), hydrogen peroxide (H_2O_2), tempol, tiron, 2-amino-2-methylpropanol hydrochloride, sodium L-lactate, D-lactate, L-glutamic acid monosodium salt hydrate (L-glutamate), β-nicotinamide adenine dinucleotide hydrate, L-lactic dehydrogenase (L-LDH), D-LDH, glutamic– pyruvate transaminase (GPT), medium 199 (M199), horseradish peroxidase (HRP)-linked goat anti-rabbit and goat anti-mouse secondary antibodies. Anti-ZO-1 rabbit polyclonal antibody and anti-occludin rabbit polyclonal antibody were obtained from Invitrogen (Carlsbad, CA, USA), anti-MG mouse monoclonal antibody was from JcICA (Fukuroi, Japan), and anti-actin mouse monoclonal antibody was from BD Biosciences (San Jose, CA, USA). HRP-linked donkey anti-rabbit and sheep anti-mouse secondary antibodies, ECL kit, and chemiluminescence detection reagents were purchased from Amersham Biopharmacia (Piscataway, NJ, USA). TRITC-conjugated donkey anti-rabbit secondary antibody was obtained from Jackson Immunoresearch Laboratories (West Grove, PA, USA). Fetal bovine serum (FBS) was purchased from Atlanta Biologicals (Atlanta, GA, USA). All other chemicals were reagent grade and purchased from Sigma.

Cell culture and cell incubations

The IHEC cell line was kindly supplied by Dr. Danica Stanimirovic of the National Research Council Canada's Institute for Biological Sciences. IHECs were cultured in M199 with 10% FBS, 1% insulin–transferrin–sodium selenite solution, and 1 × antibiotic/antimycotic at 37 °C in 5% CO_2 for 5 days. Before experiments, M199 was replaced with Hanks' balanced salt solution (HBSS) containing 25 mM Hepes and 0.5% bovine serum albumin (BSA; pH 7.35).

The following conditions were used in the various studies. IHECs (3×10^4) were cultured on 8-μm inserts in 24-well plates in full medium in studies of cell permeability and transendothelial electrical resistance (TEER), and 3×10^4 IHECs were cultured in 96-well plates in full medium in assays of ROS. In studies of GSH/GSSG, immunoprecipitation, and Western blot analyses, IHECs were cultured at 0.87×10^6 in 6-well plates in complete medium. In each instance, cells at confluency were used for experimentation (5 days postseeding). In experiments in which NAC or BSO was used to promote or inhibit GSH synthesis, respectively, cells were first pretreated overnight with 1 mM NAC or 50 μM BSO. Additionally, 2 mM NAC or 300 μM BSO was present throughout the experiment to maintain high or low cellular GSH status. To study the effect of tempol and tiron on ROS generation, cells were pretreated with 1 mM tempol or 10 mM tiron for 1 h before the

experiment, followed by the addition of the ROS scavengers at the same concentrations during cell incubations.

Assessment of IHEC barrier dysfunction

MG-mediated changes in IHEC barrier function were determined by leakage of different-sized fluorescence tracers, FITC or FITC–Dextran 150 (FITC-150, 150 kDa), and TEER.

Monolayer solute permeability

To determine monolayer solute permeability, the medium in the upper compartment of inserts was replaced with HBSS containing FITC-tagged tracers of different molecular sizes, viz., FITC (~390 Da) and FITC-150 (150 kDa). The lower chambers contained HBSS alone. IHEC monolayers were allowed to adjust to HBSS for 1 h; thereafter cells were treated with various doses of MG (0, 100 μM, 300 μM, 600 μM, and 1 mM) without or with NAC or BSO (described above). At various time points (0, 0.5, 1, 2, 3, 4, 5, and 6 h), 50-μl aliquots were sampled from the lower compartment and transferred to 96-well plates and the fluorescence was measured using a fluorimeter at excitation/emission wavelengths of 485 nm/520 nm.

Transendothelial electrical resistance

TEER studies were performed in HBSS containing 25 mM Hepes and 0.5% BSA (pH 7.35) at 37 °C and 5% CO_2. After an initial 1 h adjustment of IHEC monolayers to the medium, changes in electrical resistance at various concentrations of MG (0–1 mM) or H_2O_2 (0,100, 200, 300, and 400 μM) without or with NAC, BSO, tempol, or tiron (as above) were recorded for up to 10 h using an epithelial voltohmmeter (EVOM, World Precision Instruments, Sarasota, FL, USA). Only inserts with a minimum baseline monolayer resistance of 200 Ω/0.33 cm^2 were used. TEER was expressed as a percentage of the baseline to account for batch-to-batch variation. There was no significant cytotoxicity at all MG or H_2O_2 doses as determined by LDH leakage over the time course of the experiments.

Quantification of GSH and GSSG

At the specified times after incubation with MG without or with NAC or BSO, cells were harvested for GSH determination. Cellular contents of GSH and GSSG were determined by high-performance liquid chromatography as we previously described [9], as modified from Reed et al. [17]. Briefly cells were lysed in 5% trichloroacetic acid and scraped into 1.5-ml microcentrifuge tubes. The acid supernatants were derivatized with 6 mM iodoacetic acid and 1% 2,4-dinitrophenyl fluorobenzene to yield the *S*-carboxymethyl and 2,4-dinitrophenyl derivatives of GSH, respectively. Separation of GSH and GSSG derivatives was performed on a 250 × 4.6-mm Alltech Lichrosorb NH2 10 μm anion-exchange column. GSH and GSSG contents were quantified by comparison to standards derivatized in the same manner. Protein pellets were dissolved in 0.1 M NaOH for protein quantitation and GSH and GSSG concentrations were expressed as nanomoles per milligram of protein.

Determination of ROS

ROS formation was measured using two probes, namely, the cell-permeative oxidant-sensitive probe DHR, which is oxidized by ROS to highly fluorescent rhodamine 123, and DHE, a sensitive superoxide probe. Monolayers of IHECs grown on 96-well plates were incubated with 5 μM DHR or 10 μM DHE in HBSS containing 25 mM Hepes and 0.5% BSA (pH 7.35) for 1 h; thereafter cells were treated with various doses of MG in the absence or presence of NAC, BSO, tempol, or tiron. At various time points (0, 1, 2, 4, 6 h), rhodamine or DHE fluorescence was determined using excitation/emission wavelengths of 485/520 and 530/640 nm, respectively.

Assay for lactate

Cellular and extracellular contents of D-lactate and L-lactate were determined in IHECs (0.6×10^6) treated with 1 mM MG in the presence or absence of NAC or BSO for 0–2 h by enzymecoupled assays [18,19]. Briefly, cells were harvested into 6% perchloric acid and acid extracts were adjusted to pH 7.4. The incubation buffer (1 ml) for D-lactate assay contained 100 ml cell extract, 3 mM NAD^+, 30 mM glutamate, 40 U/ml D-LDH, 8 U/ml GPT, and propanol buffer (pH 10), and that for L-lactate contained 25 μl cell extract, 1.5 mM NAD^+, 50 mM glutamate, 40 U/ml L-LDH, 8 U/ml GPT, and 206 mM glycylglycine buffer (pH 10). Reactions were performed at 37 °C for 1 h, and NADH formation (stoichiometric with D- or L-lactate levels) was monitored spectrophotometrically at 340 nm.

Western blot analysis of cell lysates

At designated times after incubation with 300 μM or 1 mM MG, IHECs were lysed in radioimmunoprecipitation assay buffer (RIPA), containing 50 mM Tris, 150 mM NaCl, 0.1% SDS, 0.5% sodium deoxycholate, 1% Triton X-100, in the presence of aprotinin, phenylmethanesulfonyl fluoride, okadaic acid, and leupeptin. Total protein (30 μg) per sample was loaded onto either 6% (for ZO-1 proteins) or 12% SDS–polyacrylamide gels and separated at 100 V followed by transfer to polyvinylidene difluoride (PVDF) membranes for 2 h at 200 mA at 4 °C. Membranes were blocked in 5% nonfat milk in 0.1 M phosphate-buffered saline (PBS), pH 7.4, at room temperature for 1 h and then incubated with rabbit anti-ZO-1 polyclonal antibody (1:1000) or rabbit anti-occludin polyclonal antibody (1:1000) or mouse anti-MG monoclonal antibody (1:1000). After being washed, the membranes were incubated in HRP-conjugated donkey anti-rabbit or sheep anti-mouse secondary antibody (1:1000) for 2 h at room temperature followed by washing and 5 min incubation with ECL reagents. The membranes were stripped and equal protein loading was determined by β-actin expression using a mouse monoclonal antibody (1:75,000).

Immunoprecipitation

Studies were performed in IHECs treated with 1 mM MG for 4 and 6 h. Cells were lysed with RIPA buffer and cell lysates were precleared with protein A–agarose beads for 1 h at 4 °C. After centrifugation, the supernatant was transferred to a new tube and 5 μg of rabbit anti-occludin or rabbit IgG (as a negative control) was added to each reaction mixture (900 μg lysate protein/reaction) followed by incubation at 4 °C overnight with rocking. Thereafter 60 μl of protein A–agarose beads was added, and the sample was incubated for an additional 6 h at 4 °C. Agarose beads were washed four times in cell lysis buffer and bound protein was eluted in 20 μl sample buffer and boiled (100 °C, 12 min). The supernatant was collected by centrifugation and loaded onto a 10% SDS–PAGE gel and blotted with anti-MG as described above.

Immunofluorescence staining for ZO-1

IHECs were cultured on glass coverslips, and at confluency, the cells were treated with 1 mM MG with or without 2 mM NAC for 6 h. Thereafter, IHECs were fixed with ice-cold acetone (3 min) and then methanol (10 min), air dried at room temperature, and then incubated with rabbit anti-ZO-1 primary antibody (1:20) overnight at 4 °C. Coverslips were washed three times (5 min each) with 0.1% milk/PBS solution with 0.02% Triton and then incubated with fluorescently labeled donkey anti-rabbit TRITC secondary antibody (1:100) at 37 °C for 4 h in the dark. Coverslips were again washed three times with 0.1% milk/PBS solution with 0.02% Triton and mounted with Vectashield containing DAPI. ZO-1 immunostaining was visualized using a Zeiss Axio Observer.Z1 fluorescence microscope and images were captured with a Zeiss AxioCam MRm CCD camera.

Assessment of occludin and glycated occludin in control and diabetic rat brain

Induction of diabetes—Diabetes was induced in 4-week-old male Wistar rats (weighing 140 to 170 g; Harlan Laboratories) with injections of streptozotocin (STZ; 60 mg/kg in sodium citrate buffer, pH 4.5). Control animals received injections of sodium citrate buffer alone. Rats were housed one per cage and received standard chow and water. Nonfasting blood glucose levels were checked via a tail vein puncture using a One Touch Ultra glucometer (LifeScan, Milpitas, CA, USA) at 6 days after STZ injection and again on the day of sacrifice at 9 weeks after STZ or citrate buffer injections. STZ-injected rats exhibiting glucose values equal to or exceeding 300 mg/dl were considered diabetic and were used in the study. Animals were sacrificed by decapitation and brains were quickly removed and processed for immunohistochemistry or Western blot analyses. All animal protocols were approved by the Institutional Animal Care and Use Committee.

Immunohistochemistry—Harvested rat brains were placed in a rat brain slicer matrix (Zivic Instruments, Pittsburgh, PA, USA) ventral side up, and 2-mm coronal sections located 8 mm from the anterior portion of the cerebrum were cut using PBS-premoistened razor blades. The sections were placed in separate vials containing 4% cold paraformaldehyde in PBS and stored at 4 °C for at least 24 h, followed by tissue dehydration (graded 70-to-100% ethanol and xylene) and paraffin infusion. From this coronal section, 3-μm slices were cut and mounted on glass slides, two or three slices per slide. Brain slices were oven-baked for 30 min at 75 °C, deparaffinized in xylene, and rehydrated by passage through a graded series of ethanol solutions (100 to 80%) and then distilled water. Thereafter tissue slices were incubated with 1.5 mg/ml serine protease at 37 °C for 10 min followed by overnight incubation at 4 °C with 5 μg/ml anti-occludin or anti-MG polyclonal antibody in antibody dilution buffer. The next day the slides were washed three times (5 min each) with 1 × ProHisto washing solution, followed by 30 min incubation in 0.3% H_2O_2 in 50% methanol to block endogenous peroxidase activity. HRP-conjugated goat anti-rabbit or goat antimouse secondary antibody (1:200) was added and incubated with the slides for 1.5 h at room temperature. Diaminobenzidine solution was applied per the manufacturer's recommendation. Brain tissues were counterstained in hematoxylin, mounted, and dried. Immunohistochemistry staining was visualized using a Nikon Diaphot microscope equipped with a Nikon D90 camera. An average of three to five different images per brain slice were photographed and five or six microvessels were counted per image to determine the percentage of vessels that were positive for occludin or MG. Coronal sections from five control and five diabetic rat brains were analyzed.

Tissue Western blot analysis—Western blot was performed as described above for IHEC cell lysates with some modifications. Briefly, rat brains were homogenized in RIPA buffer by passing through an 18-gauge needle followed by homogenization with a polytron (10 pulses). Tissue homogenates were centrifuged at 14,000 rpm for 10 min at 4 1C, and the supernatants, representing whole-brain lysates, were used for Western blot analyses. Thirty micrograms of protein per sample was loaded onto 10% SDS–polyacrylamide gels, and electrophoresis was performed at 110 V for 2 h. Subsequent protein transfer onto PVDF membranes, blocking with nonfat milk, and incubations with anti-MG or anti-occludin antibodies were similar to those described above for IHEC cell lysates.

Protein assay

Protein concentration was determined using the Bio-Rad protein assay kit (Bio-Rad Laboratories, Hercules, CA, USA) according to the manufacturer's protocol.

Statistical analysis

Data from all experiments were analyzed by one-way ANOVA using Bonferroni's posttest for comparison of sample groups. $p < 0.05$ was considered statistically significant. Results are expressed as the mean ± SEM for 3 or 4 separate cell preparations for determinations of TEER, permeability, GSH, D-lactate, and L-lactate; 6 to 12 preparations for assay of ROS; and 3 to 5 preparations for Western blot analyses.

Results

MG induces brain endothelial barrier dysfunction that is coincident with formation of MG–occludin adducts and prevented by NAC

Fig. 2A shows that MG elicited dose- and time-dependent increases in FITC-150 leakage in IHEC monolayers, consistent with increased solute permeability. The extent of endothelial permeability to smaller sized FITC (390 Da) was greater (Fig. 2B), indicating that pathophysiologic concentrations of MG induced severe IHEC barrier dysfunction to small- and large-molecular-weight species. Coincidently, MG used at doses that mediated permeability also induced significant loss of TEER from 4 to 10 h (Fig. 2C), indicating that increased solute permeability and disruption of barrier electrical resistance were closely associated events.

The integrity of occludin and accessory ZO proteins is pivotal in maintaining high electrical resistance of brain endothelial monolayers (Fig. 3A) [12]. Therefore, increased solute permeability and loss of TEER would reflect a disruption or destabilization of tight-junction organization. Because MG is a glycating agent [20], we determined the presence of MG-glycated proteins. Fig. 3B shows that MG induced time-dependent formation of MG adducts in two distinct proteins of molecular size 130 and 65 kDa (left), consistent with increased protein glycation. Notably, the 65-kDa protein band corresponded to occludin (Fig. 3B, right). Occludin– MG adduct formation was significantly increased at 24 h, which was prevented by pretreatment of cells with NAC (Fig. 3C). To confirm the formation of the MG–occludin adduct, total cellular occludin was immunoprecipitated with anti-occludin antibody followed by blotting with anti-MG. Fig. 3D shows a single MG-positive band at 4 and 6 h in MG-treated IHECs that was quantitatively higher than in control cells. MG did not alter occludin expression (Fig. 3E). These data suggest that occludin is a target of MG modification and that occludin glycation may be a mechanism in MG-induced loss of barrier integrity. The 130-kDa glycated protein has not yet been identified.

Because occludin–ZO protein interactions are central to barrier preservation (Fig. 3A), we examined whether MG also affected ZO-1. A ZO-1 (225 kDa)–MG adduct was not detectable (Fig. 3B) and ZO-1 protein content was unchanged by MG (Fig. 3E). However, ZO-1 distribution along the periphery of IHECs was disrupted after MG treatment for 6 h (Fig. 4). NAC alone did not affect ZO-1 localization, but NAC pretreatment completely preserved ZO-1 junctional organization post-MG exposure. We also examined occludin distribution, but a demonstration of occludin association at cell junctions proved to be a challenge. The quality of the occludin antibody for immunostaining may be an issue or it may be that IHECs, like bEND.3, another immortalized brain microvascular endothelial cell line, do not exhibit distinct cell junctional localization of occludin [21].

Exogenous H_2O_2 induces endothelial barrier dysfunction, but endogenous ROS generation is not linked to MG-induced loss of barrier function

We next examined the possibility that MG-induced superoxide anion formation (Fig. 1) [6] could contribute to endothelial barrier dysfunction. Fig. 5A shows that TEER was time- and dose-dependently decreased by exogenously administered H_2O_2, a model ROS. Significant

loss of TEER was achieved at 300 and 400 μM H_2O_2 (2–6 h), indicating that ROS can disrupt IHEC barrier integrity at moderately high concentrations. The ROS levels associated with 400 μM H_2O_2 were significantly, though not completely, blocked by tempol or tiron (Fig. 5B), but these ROS scavengers significantly attenuated H_2O_2-induced TEER loss (Fig. 5C). Interestingly, for reasons yet unclear, barrier protection by tiron was more effective at earlier (1–3 h) and tempol was effective at later times (3–6 h) post-H_2O_2 treatment.

We next determined if MG caused ROS production and whether these ROS mediated IHEC barrier dysfunction. Fig. 5D shows that MG at 1 mM elicited significant DHR oxidation at 6 h that was attenuated by tiron and tempol, consistent with ROS formation. However, the extent of MG-induced ROS formation was substantially lower than 10 μM H_2O_2 (Fig. 5D), consistent with low endogenous ROS production even at this MG level. Using DHR as well as DHE as a ROS probe, we found that MG did not elicit significant DHR or DHE oxidation compared to H_2O_2 (DHR oxidation) or a superoxide generator, menadione (DHE oxidation) (Fig. 5E), in agreement with minimal ROS formation caused by MG. Accordingly, pretreatment with tiron and tempol did not prevent MG-induced TEER loss, indicating that MG-mediated barrier dysfunction was not caused by endogenously generated ROS under these conditions (Fig. 5F).

MG mediates early loss of endothelial GSH levels, and MG-induced TEER disruption is exacerbated or prevented by inhibition or promotion of GSH synthesis

The finding that MG–protein adduct formation was prevented by NAC suggests a role for GSH in barrier maintenance. To examine this, we first determined the intracellular GSH levels after MG treatment and the influence of BSO or NAC. As shown in Fig. 6A, MG significantly decreased cellular GSH at 2 h, a time point that preceded the loss of barrier function at 4 h (see Fig. 2). A 300 μM MG dose that did not elicit barrier dysfunction also did not alter cellular GSH status, supporting the idea that loss of cellular GSH was an early event that could contribute to barrier disruption induced by MG. Cellular levels of GSSG were not altered under these conditions (Fig. 6C), indicating a lack of oxidative stress. Pretreatment of cells with NAC elevated cellular GSH to levels that were higher than those in MG-treated cells (Fig. 6B) without changes in GSSG levels (Fig. 6D). This indicates that NAC treatment caused net increases in GSH production. In contrast, BSO caused an overall loss in the total cellular GSH and GSSG pools beyond the decrease induced by MG (Figs. 6B and 6D), which is consistent with a significant reduction in intracellular GSH synthetic capacity.

Fig. 7 illustrates the relationship between MG-induced IHEC barrier dysfunction and cellular GSH status as manipulated by BSO or NAC. As shown in Fig. 7A, IHEC permeability to FITC-150 induced by 1 mM MG was blunted by NAC and exacerbated by BSO. The presence of BSO potentiated IHEC barrier permeability to FITC-150 at 300 μM MG (Fig. 7B), a dose that, per se, did not increase solute permeativity (Fig. 2A). Similarly, MG-mediated TEER loss was significantly exacerbated by BSO, achieving significance as early as 2 h, whereas the level of TEER was preserved by NAC (Fig. 7C). Importantly, the protective effect of NAC was prevented by BSO (Fig. 7C), confirming that NAC served as a GSH precursor in GSH synthesis.

Endothelial GSH status is important in cellular MG metabolism

Because MG-induced barrier dysfunction was sensitive to agents that altered cellular GSH (Fig. 7), and NAC prevented MG protein glycation (Fig. 3), we examined the importance of the GSH-dependent glyoxalase system (Fig. 8A) in determining MG availability. Fig. 8B shows that cellular d-lactate production was rapid within 30 min and decayed to near baseline levels by 2 h. Moreover, d-lactate formation was significantly decreased by BSO

treatment and increased by NAC, indicating that MG was effectively metabolized by GSH-dependent glyoxalase I. Concurrent with decreased cellular D-lactate was its accumulation in the extracellular medium, which accounted for > 97% of the total produced (Fig. 8C), consistent with major metabolite export. At 1 h, ~70% of the MG administered was metabolized, a percentage that was increased by NAC (> 80%) and attenuated by BSO (~60%) (Fig. 8D). Under these conditions, MG-derived l-lactate was low regardless of the presence NAC or BSO (data not shown), suggesting a minimal involvement of the MG reductase/aldehyde dehydrogenase pathway in MG metabolism (Fig. 8A). The lack of changes in l-lactate (the physiological metabolite of glycolysis) further suggests that MG did not have a major effect on the metabolic and/or bioenergetic status of the cells under these conditions.

Diabetic rat brain microvessels are associated with decreased occludin content and increased protein glycation

Given that occludin glycation and endothelial barrier dysfunction in IHEC cultures were elicited at supraphysiological MG concentrations, we determined if protein glycation can occur in vivo in physiological conditions, such as in diabetes, a condition that is characterized by systemic hyperglycemia and elevated advanced glycation end products [22]. Brain expression of occludin and glycated adducts were examined by immunohistochemistry in STZ-induced diabetic rats. As shown in Fig. 9A, diabetic brains displayed 30% less occludin-positive but 40% higher MG-positive microvessels compared to nondiabetic brains. Western blot analyses of whole-brain homogenates confirm that the expression of occludin was attenuated (30%), whereas the ratio of glycated occludin to total occludin was significantly elevated (50%) in diabetic brains. These results suggest that occludin modification by carbonyl stress in diabetes is a physiologically relevant process in the cerebral microvasculature in vivo.

Discussion

This study provides novel evidence that MG, a model RCS, can induce glycation of the tight-junctional protein occludin in brain microvascular endothelial cells in culture, as well as in cerebral microvessels, in diabetic rat brain in vivo. In IHECs, MG-induced occludin glycation and ZO-1 disruption paralleled endothelial barrier dysfunction, a process that is sensitive to cellular GSH status. The findings that (a) MG-induced barrier failure was preceded by marked decreases in cellular GSH, (b) manipulation of cellular GSH content via inhibition or induction of GSH synthesis modified the kinetics and magnitude of MG-induced barrier dysfunction, and (c) the preservation of the endothelial barrier by NAC was preceded by NAC prevention of MG-adduct formation demonstrate that GSH has a major role in endothelial barrier integrity and that MG-induced cellular GSH loss was an early event that occurred before evidence of barrier dysfunction. Although MG also promoted ROS formation, the level of ROS produced was quantitatively low, and the lack of an effect of tempol and tiron suggests a minimal role for endogenous ROS in endothelial barrier dysfunction.

Previously we have demonstrated that IHEC apoptosis caused by MG also closely paralleled MG-mediated disruption of endothelial GSH redox balance [11]. However, MG induction of cellular GSH imbalance is not limited to endothelial cells. MG-induced decreases in GSH as well as in GSH-dependent enzymes, such as GSSG reductase and GSH *S*-transferase, have been demonstrated in rat vascular smooth muscle cells [23] and even in plant cells [24], indicating a common cross-species effect of MG in cellular GSH disruption. Our data are consistent with the notion that MG-associated consumption of cellular GSH is the result of glyoxalase I-catalyzed MG metabolism (Fig. 8A). Moreover, cellular GSH supply or store, and not altered enzyme activity, seems to be a determinant in the availability of MG for

MG–protein crosslink reactions. Although MG has been shown to decrease glyoxalase I and II activities through posttranslational protein modification [25], our results showing that D-lactate formation accounted for >80% of the administered MG dose (Fig. 8) are consistent with active enzyme function. Because the glyoxalase system accounts for >90% of intracellular MG removal [26], decreased GSH, such as with BSO treatment, is expected to result in enhanced MG availability for glycation reactions.

Significantly, the tight-junctional proteins occludin and ZO-1 were respectively targets of protein glycation or disruption, both of which were prevented by NAC (Figs. 3 and 4). Neither protein level was altered by MG. Previous studies have shown that oxidants such as H_2O_2, peroxynitrite, and superoxide decreased the expression of ZO-1 and occludin and disrupted their architectural organization [27–29]. Moreover, H_2O_2 exposure was shown to redistribute occludin and dissociate it from ZO-1 [27]. A loss of the expression of these proteins has been linked to an increase in BBB permeability in diabetes [30]. As a glycating agent, MG can react irreversibly with free arginine residues of proteins, which results in the formation of advanced glycated end products [20]. MG-derived argpyrimidine has been detected in human lens and kidney, in atherosclerotic lesions of diabetic patients, and in familial amyloidotic polyneuropathy [31–35]. In endothelial cells, the heat shock protein 27 is a major argpyrimidine-modified protein and is a contributor to altered endothelial cell function in diabetes [36].

The potential sites of occludin chemical modification are unknown. We infer from the lack of ZO-1–MG adduct formation that MG–occludin glycation probably occurs outside of cells. We previously found that the LYHY (leucine-tyrosine-histidine-tyrosine) motif represents an important intercellular adhesion recognition sequence in the second extracellular loop of occludin, which mediates barrier function [37]. Given the recent discovery that l-leucine can react with MG to form a stable ketoamine [38], the leucine in the LYHY sequence would probably be susceptible to modification by MG. Moreover, we found that experimental blockade of the LYHY motif using a cyclized peptide containing this sequence disturbed junction-mediated barrier integrity. Therefore, junctional disruption and loss of barrier function could result from MG-induced chemical modification of the LYHY sequence of occludin. Interestingly, although occludin is important in establishing and maintaining tight junctions [39], the knockdown of occludin in animal models did not adversely affect endothelial barrier function. For reasons yet unclear, occludin-null mice exhibited only minor alterations in barrier function [40]. One possible explanation may be that genetic deletion of the occludin gene could result in an altered phenotype compared to the wild type. Indeed, we have demonstrated that pharmacologic modification of the native occludin LYHY binding motif in wild-type rats by subcutaneous administration of a cyclized peptide bearing this sequence can induce a loss of barrier function [37].

Importantly, the results of this study suggest that carbonyl stress-induced tight-junctional disruption could be a mechanism in barrier impairment associated with vascular pathology, such as in diabetes [41,42]. Because IHECs functionally exhibit BBB properties [43], and are a reasonable model for the BBB in vivo, our results may be meaningful for understanding BBB endothelial response to systemic carbonyl stress. We recognize that the physiological relevance of our findings in IHEC cultures is limited by the supraphysiological levels of MG that were needed to induce microvascular permeability, a common concern in cell culture studies. However, the studies in diabetic rats demonstrated that the cerebral microvasculature was, in fact, affected in diabetes. Notably, diabetic rat brains exhibited two features that were distinct from control brains, namely, (a) lower total occludin levels and smaller number of occludin-positive cerebral micro-vessels and (b) higher percentage of MG-positive microvessels and elevated glycated occludin. This means that the threshold for eliciting brain microvascular pathology in vivo during the diabetic

state could be achieved at physiologically relevant systemic MG levels. Very likely, carbonyl stress-mediated cerebral endothelial barrier dysfunction in vivo is modulated by other factors, such as the presence of astrocytes, a major pervascular cell in the brain capillary neurovascular unit of the BBB [12]; the hyperglycemic state and hence sustained generation of MG in the local environment of the endothelium; or diabetes-associated decrease in endothelial GSH [44]. It has been documented that a dose of 5 μM MG coupled with high glucose (15–30 mM) can induce apoptosis and necrosis in endothelial and mononuclear cells [45,46]. In ongoing studies, we similarly found that hyperglycemia (25 mM glucose, 5 days) can sensitize IHECs to MG-induced TEER loss (greater than fivefold), perhaps by lowering the MG threshold in mediating barrier dysfunction.

Decreased occludin levels have been reported in the cerebral microvasculature of type 2 diabetic rats [47] and diabetic rat retina [48,49]; interestingly, the latter was temporally associated with an increase in blood–retinal barrier permeability [48]. The mechanism of endothelial occludin decrease is unknown. In retinal endothelial cells, a role for VEGF was implicated in occludin decrease, whereas insulin was shown to reverse occludin loss [48,49]. Here, a novel finding is diabetes-associated elevated protein (occludin) glycation in cerebral microvessels. At present, the biological significance of protein glycation in diabetic cerebral microvascular pathology is unclear and warrants further investigation. Previous studies have detected glycated protein adducts in the arterial wall of the large middle cerebral artery after occlusion and reperfusion [31], but it remains unclear whether protein adduct formation affects stroke outcome.

In summary, this study has provided new insights into the relationship between carbonyl stress and brain microvascular endothelial barrier function and the role of GSH. This information could have important implications for the pathophysiologic state of diabetes and other degenerative disorders that are associated with systemic or elevated carbonyl stress. And, MG-lowering agents could offer a promising therapeutic strategy under these conditions.

Acknowledgments

We thank Vijay Ganta and Merilyn Jennings for assistance in the TEER experiments. We also thank Dr. Norman Harris for assistance with the diabetic rat model and Christopher Monceaux and Georgia Morgan for help with immunohistochemistry and immunofluorescence microscopy, respectively. This work was supported by NIH Grant DK44510 (T.Y.A.) and by an LSUHSC Malcolm Feist Cardiovascular Fellowship (W.L.).

References

1. Madamanchi NR, Vendrov A, Runge MS. Oxidative stress and vascular disease. Arterioscler Thromb Vasc Biol. 2005; 25:29–38. [PubMed: 15539615]
2. Stitt AW, Jenkins AJ, Cooper ME. Advanced glycation end products and diabetic complications. Expert Opin Invest Drugs. 2002; 11:1205–1223.
3. Akhand AA, Kato M, Suzuki H, Liu W, Du J, Hamaguchi M, Miyata T, Kurokawa K, Nakashima I. Carbonyl compounds crosslink cellular proteins and activate protein-tyrosine kinase p60c-Src. J Cell Biochem. 1999; 72:1–7. [PubMed: 10025661]
4. Rosca MG, Monnier VM, Szweda LI, Weiss MF. Alterations in renal mitochondrial respiration in response to the reactive oxoaldehyde methylglyoxal. Am J Physiol Renal Physiol. 2002; 283:F52–F59. [PubMed: 12060586]
5. Akhand AA, Hossain K, Mitsui H, Kato M, Miyata T, Inagi R, Du J, Takeda K, Kawamoto Y, Suzuki H, Kurokawa K, Nakashima I. Glyoxal and methylglyoxal trigger distinct signals for MAP family kinases and caspase activation in human endothelial cells. Free Radic Biol Med. 2001; 31:20–30. [PubMed: 11425486]

6. Yim HS, Kang SO, Hah YC, Chock PB, Yim MB. Free radicals generated during the glycation reaction of amino acids by methylglyoxal: a model study of protein-cross-linked free radicals. J Biol Chem. 1995; 270:28228–28233. [PubMed: 7499318]
7. Duran-Jimenez B, Dobler D, Moffatt S, Rabbani N, Streuli CH, Thornalley PJ, Tomlinson DR, Gardiner NJ. Advanced glycation endproducts in extracellular matrix proteins contribute to the failure of sensory nerve regeneration in diabetes. Diabetes. 2009; 58:2893–2903. [PubMed: 19720799]
8. Ota K, Nakamura J, Li W, Kozakae M, Watarai A, Nakamura N, Yasuda Y, Nakashima E, Naruse K, Watabe K, Kato K, Oiso Y, Hamada Y. Metformin prevents methylglyoxal-induced apoptosis of mouse Schwann cells. Biochem Biophys Res Commun. 2007; 357:270–275. [PubMed: 17418096]
9. Okouchi M, Okayama N, Aw TY. Differential susceptibility of naive and differentiated PC-12 cells to methylglyoxal-induced apoptosis: influence of cellular redox. Curr Neurovasc Res. 2005; 2:13–22. [PubMed: 16181096]
10. Jan CR, Chen CH, Wang SC, Kuo SY. Effect of methylglyoxal on intracellular calcium levels and viability in renal tubular cells. Cell Signalling. 2005; 17:847–855. [PubMed: 15763427]
11. Okouchi M, Okayama N, Aw TY. Preservation of cellular glutathione status and mitochondrial membrane potential by N-acetylcysteine and insulin sensitizers prevent carbonyl stress-induced human brain endothelial cell apoptosis. Curr Neurovasc Res. 2009; 6:267–278. [PubMed: 19807652]
12. Hawkins BT, Davis TP. The blood–brain barrier/neurovascular unit in health and disease. Pharmacol Rev. 2005; 57:173–185. [PubMed: 15914466]
13. Townsend DM, Tew KD, Tapiero H. The importance of glutathione in human disease. Biomed Pharmacother. 2003; 57:145–155. [PubMed: 12818476]
14. Rose IA, Nowick JS. Methylglyoxal synthetase, enolpyruvaldehyde, glutathione and the glyoxalase system. J Am Chem Soc. 2002; 124:13047–13052. [PubMed: 12405831]
15. Thornalley PJ. Protein and nucleotide damage by glyoxal and methylglyoxal in physiological systems—role in ageing and disease. Drug Metab Drug Interact. 2008; 23:125–150.
16. Kaplowitz N, Aw TY, Ookhtens M. The regulation of hepatic glutathione. Annu Rev Pharmacol Toxicol. 1985; 25:715–744. [PubMed: 3890714]
17. Reed DJ, Babson JR, Beatty PW, Brodie AE, Ellis WW, Potter DW. High-performance liquid chromatography analysis of nanomole levels of glutathione, glutathione disulfide, and related thiols and disulfides. Anal Biochem. 1980; 106:55–62. [PubMed: 7416469]
18. Lowry, O. H., Passoneau, J. V., editors. New York: Academic Press; 1972.
19. Martı R, Varela E, Segura RM, Alegre J, Suriñach JM, Pascual C. Determination of D-lactate by enzymatic methods in biological fluids: study of interferences. Clin Chem. 1997; 43:1010–1015. [PubMed: 9191554]
20. Lo TW, Westwood ME, McLellan AC, Selwood T, Thornalley PJ. Binding and modification of proteins by methylglyoxal under physiological conditions: a kinetic and mechanistic study with N alpha-acetylarginine, N alpha-acetylcysteine, and N alpha-acetyllysine, and bovine serum albumin. J Biol Chem. 1994; 269:32299–322305. [PubMed: 7798230]
21. Song L, Pachter JS. Culture of murine brain microvascular endothelial cells that maintain expression and cytoskeletal association of tight junctionassociated proteins. In Vitro Cell Dev Biol Anim. 2003; 39:313–320. [PubMed: 14613336]
22. Aso Y, Inukai T, Tayama K, Takemura Y. Serum concentrations of advanced glycation endproducts are associated with the development of atherosclerosis as well as diabetic microangiopathy in patients with type 2 diabetes. Acta Diabetol. 2000; 37:87–92. [PubMed: 11194933]
23. Wu L, Juurlink BH. Increased methylglyoxal and oxidative stress in hypertensive rat vascular smooth muscle cells. Hypertension. 2002; 39:809–814. [PubMed: 11897769]
24. Hoque MA, Uraji M, Banu MN, Mori IC, Nakamura Y, Murata Y. The effects of methylglyoxal on glutathione S-transferase from Nicotiana tabacum. Biosci Biotechnol Biochem. 2010; 74:2124–2126. [PubMed: 20944411]

25. Di Loreto S, Zimmitti V, Sebastiani P, Cervelli C, Falone S, Amicarelli F. Methylglyoxal causes strong weakening of detoxifying capacity and apoptotic cell death in rat hippocampal neurons. Int J Biochem Cell Biol. 2008; 40:245–257. [PubMed: 17869161]
26. Ghoshal K, Banerjee AB, Ray S. Methylglyoxal-catabolizing enzymes of Leishmania donovani promastigotes. Mol Biochem Parasitol. 1989; 35:21–29. [PubMed: 2668758]
27. Kevil CG, Oshima T, Alexander B, Coe LL, Alexander JS. H_2O_2-mediated permeability: role of MAPK and occludin. Am J Physiol Cell Physiol. 2000; 279:C21–C30. [PubMed: 10898713]
28. Mazzon E, De Sarro A, Caputi AP, Cuzzocrea S. Role of tight junction derangement in the endothelial dysfunction elicited by exogenous and endogenous peroxynitrite and poly(ADP-ribose) synthetase. Shock. 2002; 18:434–439. [PubMed: 12412622]
29. Zhang Y, Zhao S, Gu Y, Lewis DF, Alexander JS, Wang Y. Effects of peroxynitrite and superoxide radicals on endothelial monolayer permeability: potential role of peroxynitrite in preeclampsia. J Soc Gynecol Invest. 2005; 12:586–592.
30. Hawkins BT, Lundeen TF, Norwood KM, Brooks HL, Egleton RD. Increased blood–brain barrier permeability and altered tight junctions in experimental diabetes in the rat: contribution of hyperglycaemia and matrix metalloproteinases. Diabetologia. 2007; 50:202–211. [PubMed: 17143608]
31. Oya T, Hattori N, Mizuno Y, Miyata S, Maeda S, Osawa T, Uchida K. Methylglyoxal modification of protein: chemical and immunochemical characterization of methylglyoxal–arginine adducts. J Biol Chem. 1999; 274:18492–18502. [PubMed: 10373458]
32. Padayatti PS, Ng AS, Uchida K, Glomb MA, Nagaraj RH. Argpyrimidine, a blue fluorophore in human lens proteins: high levels in brunescent cataractous lenses. Invest Ophthalmol Visual Sci. 2001; 42:1299–1304. [PubMed: 11328743]
33. Raj DS, Lim G, Levi M, Qualls C, Jain SK. Advanced glycation end products and oxidative stress are increased in chronic allograft nephropathy. Am J Kidney Dis. 2004; 43:154–160. [PubMed: 14712439]
34. Baba SP, Barski OA, Ahmed Y, O'Toole TE, Conklin DJ, Bhatnagar A, Srivastava S. Reductive metabolism of AGE precursors: a metabolic route for preventing AGE accumulation in cardiovascular tissue. Diabetes. 2009; 58:2486–2497. [PubMed: 19651811]
35. Gomes R, Sousa Silva M, Quintas A, Cordeiro C, Freire A, Pereira P, Martins A, Monteiro E, Barroso E, Ponces Freire A. Argpyrimidine, a methylglyoxal-derived advanced glycation end-product in familial amyloidotic polyneuropathy. Biochem J. 2005; 385:339–345. [PubMed: 15281912]
36. Schalkwijk CG, van Bezu J, van der Schors RC, Uchida K, Stehouwer CD, van Hinsbergh VW. Heat-shock protein 27 is a major methylglyoxal-modified protein in endothelial cells. FEBS Lett. 2006; 580:1565–1570. [PubMed: 16487519]
37. Blaschuk OW, Oshima T, Gour BJ, Symonds JM, Park JH, Kevil CG, Trocha SD, Michaud S, Okayama N, Elrod JW, Alexander JS. Identification of an occludin cell adhesion recognition sequence. Inflammation. 2002; 26:193–198. [PubMed: 12184633]
38. Suravajjala, S. Non-enzymatic glycation of bio-molecules by sugars and sugar metabolites. Dissertation and Master's Theses, University of Rhode Island. http://digitalcommons.uri.edu/dissertations/AAI3503574, in press
39. Murata M, Kojima T, Yamamoto T, Go M, Takano K, Osanai M, Chiba H, Sawada N. Down-regulation of survival signaling through MAPK and Akt in occludin-deficient mouse hepatocytes in vitro. Exp Cell Res. 2005; 310:140–151. [PubMed: 16112666]
40. Saitou M, Furuse M, Sasaki H, Schulzke JD, Fromm M, Takano H, Noda T, Tsukita S. Complex phenotype of mice lacking occludin, a component of tight junction strands. Mol Biol Cell. 2000; 11:4131–4142. [PubMed: 11102513]
41. Lapolla A, Flamini R, Dalla Vedova A, Senesi A, Reitano R, Fedele D, Basso E, Seraglia R, Traldi P. Glyoxal and methylglyoxal levels in diabetic patients: quantitative determination by a new GC/MS method. Clin Chem Lab Med. 2003; 41:1166–1173. [PubMed: 14598866]
42. Beisswenger PJ, Howell SK, Touchette AD, Lal S, Szwergold BS. Metformin reduces systemic methylglyoxal levels in type 2 diabetes. Diabetes. 1999; 48:198–202. [PubMed: 9892243]

43. Sharp CD, Hines I, Houghton J, Warren A, Jackson TH 4th, Jawahar A, Nanda A, Elrod JW, Long A, Chi A, Minagar A, Alexander JS. Glutamate causes a loss in human cerebral endothelial barrier integrity through activation of NMDA receptor. Am J Physiol Heart Circ Physiol. 2003; 285:H2592–H2598. [PubMed: 12893641]
44. Soliman GZ. Blood lipid peroxidation (superoxide dismutase, malondialdehyde, glutathione) levels in Egyptian type 2 diabetic patients. Singapore Med J. 2008; 49:129–136. [PubMed: 18301840]
45. Chan WH, Wu HJ. Methylglyoxal and high glucose co-treatment induces apoptosis or necrosis in human umbilical vein endothelial cells. J Cell Biochem. 2008; 103:1144–1157. [PubMed: 17721990]
46. Hsieh MS, Chan WH. Impact of methylglyoxal and high glucose cotreatment on human mononuclear cells. Int J Mol Sci. 2009; 10:1445–1464. [PubMed: 19468318]
47. Li W, Prakash R, Kelly-Cobbs AI, Ogbi S, Kozak A, El-Remessy AB, Schreihofer DA, Fagan SC, Ergul A. Adaptive cerebral neovascularization in a model of type 2 diabetes: relevance to focal cerebral ischemia. Diabetes. 2010; 59:228–235. [PubMed: 19808897]
48. Antonetti DA, Barber AJ, Khin S, Lieth E, Tarbell JM, Gardner TW. Vascular permeability in experimental diabetes is associated with reduced endothelial occludin content: vascular endothelial growth factor decreases occludin in retinal endothelial cells. Penn State Retina Research Group. Diabetes. 1998; 47:1953–1959. [PubMed: 9836530]
49. Barber AJ, Antonetti DA, Gardner TW. Altered expression of retinal occludin and glial fibrillary acidic protein in experimental diabetes. Penn State Retina Research Group. Invest Ophthalmol Visual Sci. 2000; 41:3561–3568. [PubMed: 11006253]
50. Shusta, EV. Blood–brain barrier. In: Aird, WC., editor. Endothelial Cells in Health and Disease. Boca Raton: Taylor & Francis; 2005. p. 33-63.

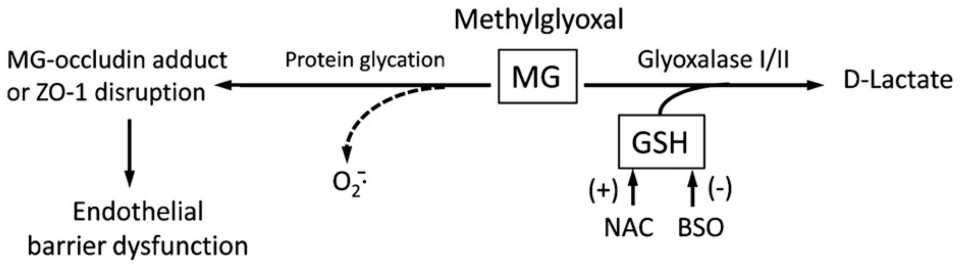

Fig. 1.

Proposed mechanism by which MG mediates endothelial barrier dysfunction and its protection by GSH. MG-induced endothelial barrier dysfunction can be caused by MG protein glycation that results in MG–occludin adduct formation or ZO-1 disruption. GSH protection of barrier integrity can occur through GSH-dependent, glyoxalase I-catalyzed metabolism of MG. The effects of NAC or BSO relate to their respective stimulation or inhibition of cellular GSH synthesis. A possibility that barrier damage may also result from ROS generation during protein glycation is indicated by the dotted line. MG, methylglyoxal; GSH, reduced glutathione; $O_2^{\cdot-}$, superoxide anion; NAC, *N*-acetylcysteine; BSO, buthionine sulfoximine.

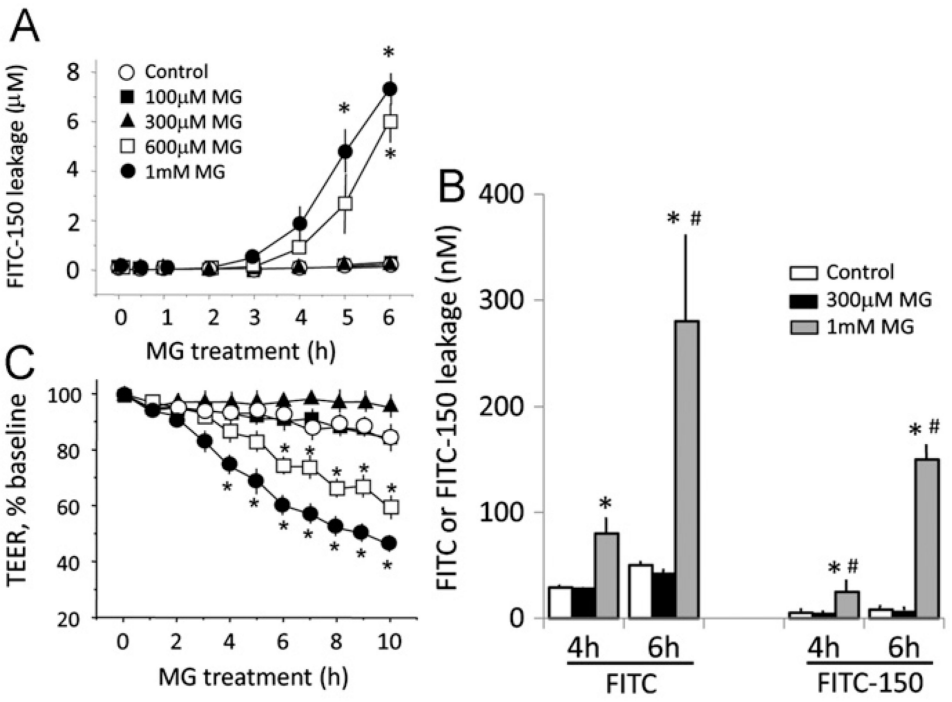

Fig. 2.

MG mediates human brain endothelial barrier dysfunction. (A) IHEC permeability to FITC-Dextran 150 (FITC-150). IHECs were exposed to 100 μM, 300 μM, 600 μM, or 1 mM MG in transwell assays. FITC-150 was added to the upper chamber and cell permeability is expressed as FITC-150 concentration in the lower chamber. *$p < 0.05$ vs control, n=4. (B) Comparison of IHEC permeability to small (FITC)- and large (FITC-150)-molecular-weight species at 4 and 6 h post-MG treatment. *$p < 0.05$ vs control, #$p < 0.05$, 1 mM MG vs 300 μM MG, n=3. (C) Loss of transendothelial electrical resistance (TEER) induced by various doses of MG. TEER changes in IHECs grown on inserts were recorded hourly for 10 h using an epithelial voltohmmeter. Only inserts with a minimum baseline monolayer resistance of 200 Ω/0.33 cm^2 were used. TEER was expressed as the percentage of the baseline to account for batch-to-batch variation. *$p < 0.05$ vs control, n=3.

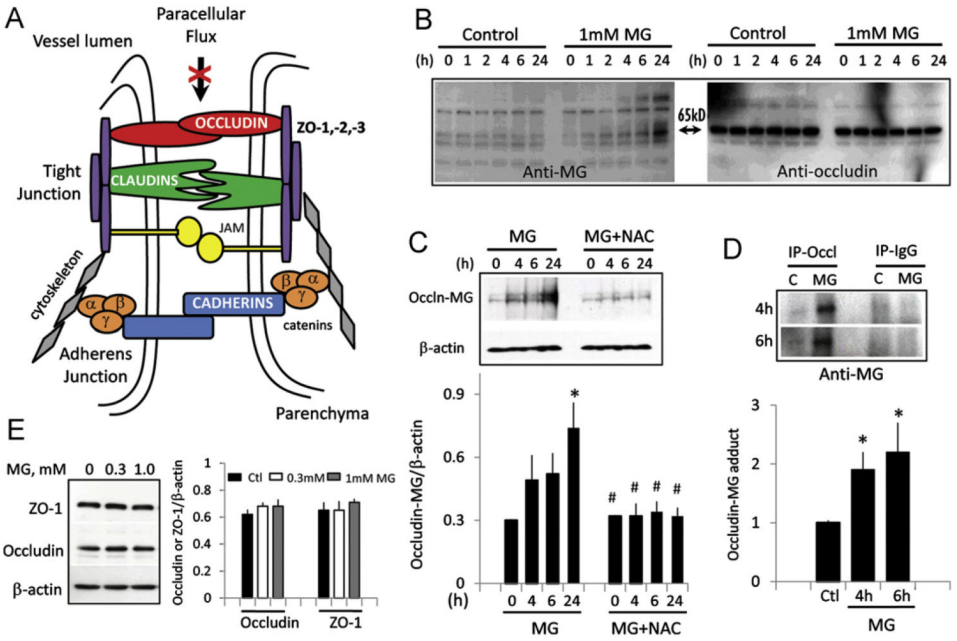

Fig. 3.

MG induces occludin glycation. (A) Schematic of architectural organization of tight-junctional proteins of capillary cell–cell junction that controls brain endothelial barrier resistance and paracellular flux. Redrawn from Shusta [50]. (B) MG-mediated time-dependent increase in glycation of proteins, including occludin. IHECs were treated with 1 mM MG for 0–24 h and total MG-protein adducts were examined in whole-cell lysates by Western blot analyses using anti-MG antibody. Left shows time-dependent increase in protein adducts, notably in proteins of molecular weights of 65 and 130 kDa. Right shows the same membrane reprobed for occludin, which corresponded to the 65-kDa band. (C) NAC attenuates occludin–MG adduct formation. IHECs were treated with 1 mM MG in the absence or presence of 2 mM NAC, and MG-adduct formation was determined at 4, 6, and 24 h by Western blot analyses. Shown below is the quantitation of band intensity relative to β-actin, mean ± SEM for six separate blots. *p <0.05 vs 0 h; #p <0.05 vs corresponding MG treatment. (D) Whole-cell extracts were prepared from IHECs treated with 1 mM MG for 4 or 6 h, and occludin was immunoprecipitated with anti-occludin antibody followed by Western blot analysis with anti-MG. IgG served as negative control. Shown below is the quantitation of occludin–MG band intensity normalized to IgG, mean ± SEM for three separate blots. *p <0.05 vs control. (E) Protein expression of ZO-1 (225 kDa) and occludin (65 kDa) in whole-cell lysates was examined after treatment of IHECs with 300 μM or 1 mM MG. Quantitation of ZO-1 and occludin contents relative to β-actin (mean ± SEM) is shown for six separate blots.

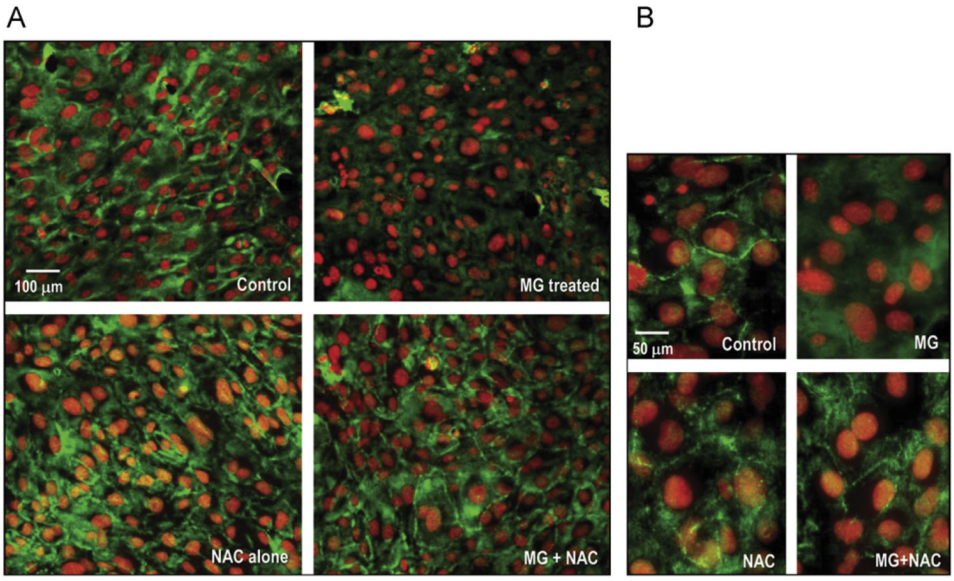

Fig. 4.

MG disrupts the architectural organization of ZO-1. (A) IHECs were grown on glass coverslips, and confluent cells were treated with 1 mM MG with or without 2 mM NAC for 6 h. Immunostaining was performed with anti-ZO-1 primary antibody and fluorescently labeled anti-rabbit TRITC secondary antibody as described under Materials and methods. Control IHECs exhibited normal ZO-1 distribution along the cell periphery, which was disrupted after MG treatment, and prevented by NAC pretreatment. Higher magnification images are shown in (B).

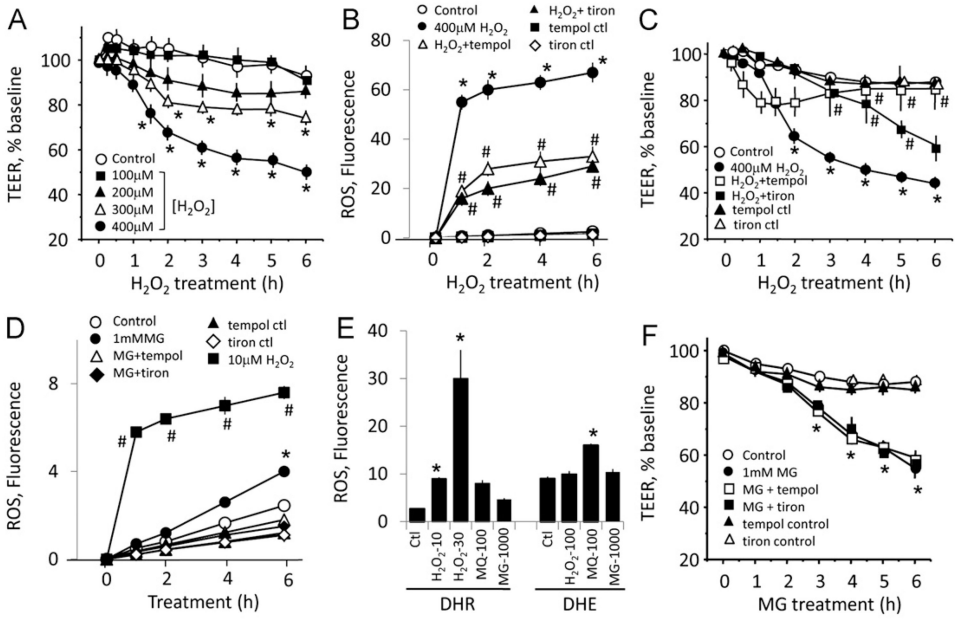

Fig. 5.

Endothelial barrier dysfunction is mediated by exogenous H_2O_2, but not by endogenous MG-induced ROS. (A) H_2O_2 induced time- and dose-dependent TEER loss. IHECs were exposed to 100, 200, 300, or 400 μM H_2O_2, and TEER was monitored for 0–6 h. *$p < 0.05$ vs control, n=4. (B) IHECs were treated with 400 μM H_2O_2 for 0–6 h in the absence or presence of 1 mM tempol or 10 mM tiron. ROS production was significantly attenuated, but not completely blocked by the ROS scavengers. *$p < 0.05$ vs control; #$p < 0.05$ vs 400 μM H_2O_2, n=6 preparations performed in quadruplicate. (C) Tempol and tiron exhibited different kinetics of protection against H_2O_2-induced TEER loss. IHECs were treated with 400 μM H_2O_2 in the absence or presence of 1 mM tempol or 10 mM tiron, and TEER was recorded for 0–6 h. *$p < 0.05$ vs control; #$p < 0.05$ vs 400 μM H_2O_2, $n = 4$. (D) MG-induced ROS were significantly lower than 10 μM H_2O_2. *$p < 0.05$ vs control, #$p < 0.05$ vs 1 mM MG, n=6 preparations performed in quadruplicate. (E) MG induced minimal ROS formation in comparison to H_2O_2 (DHR oxidation) or a superoxide generator, menadione (MQ; DHE oxidation). The numbers associated with H_2O_2, MQ, and MG represent their concentrations in μM. *$p < 0.05$ vs control, $n = 6$ preparations performed in quadruplicate. (F) MG-induced ROS did not mediate TEER changes. IHECs were pretreated with tempol or tiron for 1 h and thereafter exposed to 1 mM MG. TEER were monitored for 0 to 6 h. *$p < 0.05$ vs control, n=3.

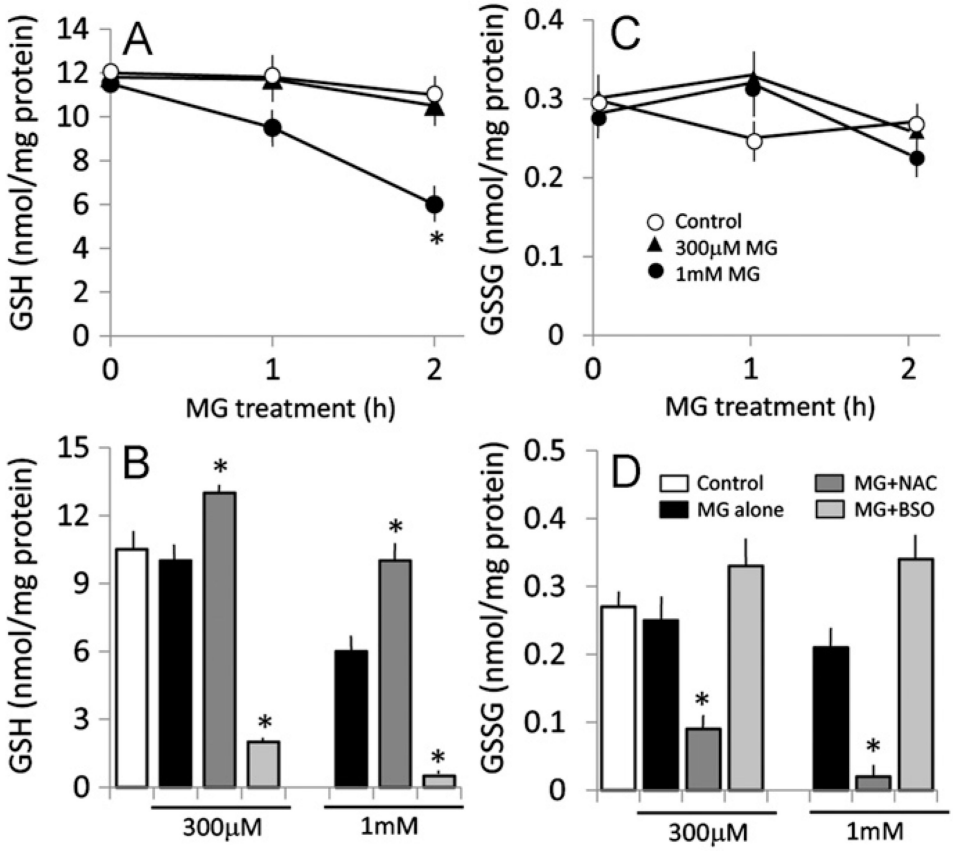

Fig. 6.

MG decreases brain endothelial GSH, which is prevented by NAC and exacerbated by BSO. IHECs were pretreated overnight with 1 mM NAC or 50 μM BSO and then challenged with 300 μM or 1 mM MG in the absence or presence of additional 2 mM NAC or 300 μM BSO. (A, C) Kinetics of MG-induced changes in endothelial GSH and GSSG. *$p < 0.05$ vs control, n=4. (B, D) MG decreased endothelial cell GSH, which was blocked or exaggerated by NAC or BSO, respectively (B). Endothelial GSSG was significantly attenuated by NAC (D). *$p < 0.05$ vs MG alone at 300 μM or 1 mM, n=4.

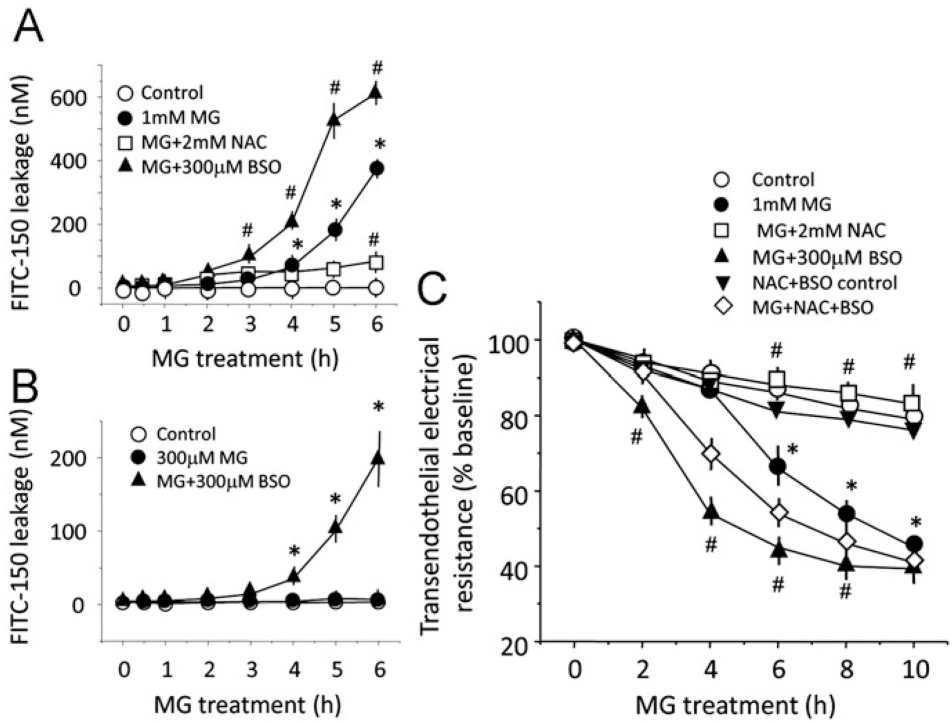

Fig. 7.

MG-mediated brain endothelial barrier dysfunction is sensitive to intracellular GSH status. IHECs were pretreated overnight with 1 mM NAC or 50 μM BSO and thereafter exposed to 300 μM or 1 mM MG in the presence of 2 mM NAC or 300 μM BSO. Permeability to FITC-150 and TEER were determined as measures of barrier function. (A) Protection or exacerbation of MG-induced FITC-150 permeativity by NAC or BSO treatment, respectively. *$p < 0.05$ vs control, #$p < 0.05$ vs 1 mM MG, n=4. (B) Potentiation of FITC-150 permeativity by BSO at 300 μM MG, a dose that did not per se increase cell permeability. *$p < 0.05$ vs control, n=3. (C) MG-induced TEER loss was prevented or exacerbated by NAC or BSO, respectively. The protective effect of NAC was blocked by BSO, consistent with NAC promoting endothelial GSH synthesis. *$p < 0.05$ vs control, #$p <$ 0.05 vs MG alone, n=3.

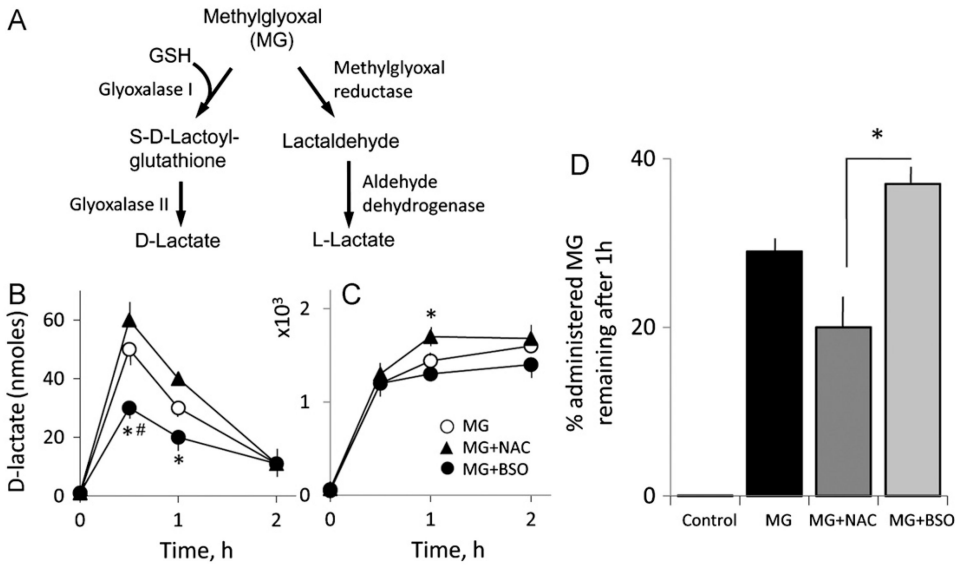

Fig. 8.

D-Lactate formation is respectively decreased or increased under conditions of inhibition or stimulation of endothelial GSH synthesis. (A) Cellular pathways of MG metabolism. MG can be metabolized by two possible pathways: (a) GSH-dependent glyoxalase I/II pathway with *S*-D-lactoylglutathione and D-lactate as the intermediate and final metabolites or (b) GSH-independent MG reductase/aldose reductase pathway with L-lactate as the final product. (B, C) Intracellular d-lactate formation (B) and its extracellular accumulation (C) were determined in IHECs treated with 1 mM MG in the absence or presence of NAC or BSO. IHEC extracts and extracellular media were obtained from 0 to 2 h, and D-lactate levels were determined by enzyme-coupled assays [18,19]. (D) Percentage of administered MG remaining after 1 h (maximal appearance in extracellular medium) in control or NAC- or BSO-treated IHECs was calculated by subtracting the nanomoles of D-lactate produced from the total nanomoles of MG added. The results are expressed as a percentage. *$p < 0.05$ vs MG+NAC; #$p < 0.05$ vs MG alone, n=3.

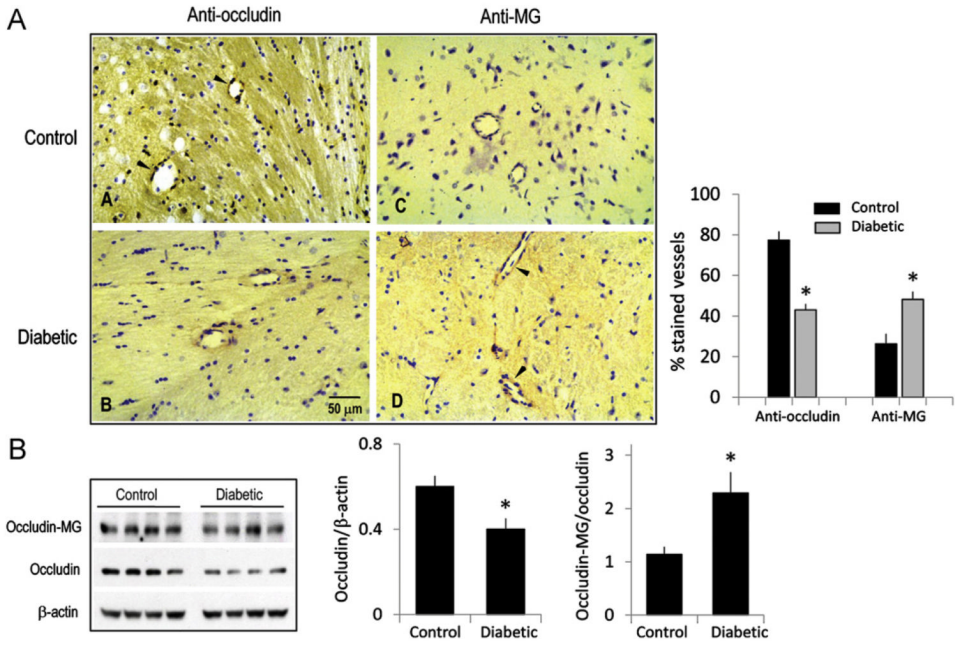

Fig. 9.

Diabetic brain is associated with decreased total occludin but increased glycated protein. (A) Immunohistochemistry of occludin and glycated protein in cerebral microvessels in diabetic rat brain. Arrowheads indicate occludin- or MG-positive cells in representative cerebral microvessels. The number of occludin- or MG-positive cerebral microvessels is expressed as a percentage of the total vessels counted as described under Methods. (B) Protein expression of occludin and MG–occludin adducts in whole brain extracts. Quantitation of protein shows a significant decrease in occludin content, but increased MG–occludin adducts compared to total occludin. Data are means ± SEM, n=5 separate immunoblots each with brain homogenates from two control or diabetic rats performed in duplicate. *$p < 0.05$ vs control.